The Journal of Physical Chemistry Letters
Letter
pubs.acs.org/JPCL

Room-Temperature Coherent Optical Phonon in 2D Electronic Spectra of $CH_3NH_3PbI_3$ Perovskite as a Possible Cooling Bottleneck

Daniele M. Monahan,[§,†,⊥] Liang Guo,[§,†,⊥] Jia Lin,[§,‡,⊥] Letian Dou,[§,‡,⊥] Peidong Yang,[§,‡,⊥] and Graham R. Fleming*[,§,†,⊥]

[§]Department of Chemistry, University of California, Berkeley, California 94720, United States
[†]Molecular Biophysics and Integrated Bioimaging Division, Lawrence Berkeley National Laboratory, Berkeley, California 94720, United States
[‡]Materials Sciences Division, Lawrence Berkeley National Laboratory, Berkeley, California 94720, United States
[⊥]Kavli Energy NanoSciences Institute at Berkeley, Berkeley, California 94720, United States

ABSTRACT: A hot phonon bottleneck may be responsible for slow hot carrier cooling in methylammonium lead iodide hybrid perovskite, creating the potential for more efficient hot carrier photovoltaics. In room-temperature 2D electronic spectra near the band edge, we observe amplitude oscillations due to a remarkably long lived 0.9 THz coherent phonon population at room temperature. This phonon (or set of phonons) is assigned to angular distortions of the Pb−I lattice, not coupled to cation rotations. The strong coupling between the electronic transition and the 0.9 THz mode(s), together with relative isolation from other phonon modes, makes it likely to cause a phonon bottleneck. The pump frequency resolution of the 2D spectra also enables independent observation of photoinduced absorptions and bleaches independently and confirms that features due to band gap renormalization are longer-lived than in transient absorption spectra.

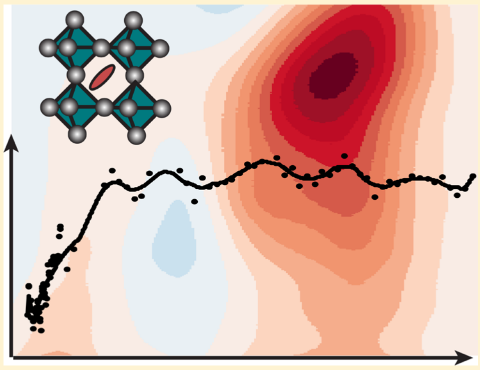

Hybrid organic−inorganic perovskites, especially methylammonium lead iodide (MAPI), have in recent years demonstrated remarkable increases in photovoltaic efficiency. Despite a soft, fluctuating structure, MAPI films exhibit an impressive set of optoelectronic properties, including microsecond carrier lifetimes, high carrier mobility, and long carrier diffusion lengths.[1−6] From the intensive study of these materials in recent years, it has become clear that fundamentally different physics are responsible for the high performance of hybrid perovskite photovoltaics as compared to more traditional solid-state semiconductor devices. In addition to their promise for solar energy, hybrid perovskites may find applications in LED, photodetector, laser,[7,8] and thermoelectric[9] devices. Because these materials are solution-processable, they are potentially quite economical. Unfortunately, MAPI's commercial applications are limited by thermodynamic instability,[10] moisture sensitivity, and lead toxicity. Understanding the principles and mechanisms behind this material's exceptional optoelectronic properties is an important step in the search for a variant material with the potential for wider application.[11]

Unlike conventional solid-state inorganic photovoltaics, MAPI is soft and polarizable. At room temperature, it has a high dielectric constant and strong Coulomb screening. This results in small exciton binding energies[12,13] and consequent rapid free carrier generation upon photoexcitation. Screening effects are also important in determining the strength of carrier−carrier and carrier−lattice interactions. Wang et al. observed a large difference in carrier lifetimes between the low-temperature orthorhombic phase of MAPI and the room-temperature tetragonal phase,[14] consistent with the changes in Coulomb screening caused by the discontinuity in the dielectric constant across this phase boundary. Zhu and co-workers proposed a "large polaron" model[15] to explain the slow recombination at room temperature. In the polaron model, the methylammonium cation rotations and/or lattice deformations rapidly respond to charge carrier generation, creating a solvation-like envelope and a barrier to recombination. Indeed, Zhu and co-workers' optical Kerr effect measurements showed liquid-like reorientation dynamics stemming from the organic cation.[16] In a recent 2D-IR study,[17] Bakulin et al. directly measured the organic cation reorientations, observing separate fast (∼0.3 ps) and slow (>2 ps) time scales. However, the extent to which the organic cation (as opposed to deformations of the inorganic lattice) might contribute to screening or polaron formation remains an open question.

The observation of persistent hot carriers[18−20] presents another intriguing prospect for hybrid perovskite photovoltaics. Paired with energy-selective electrical contacts, such a material could be used to make a hot carrier solar cell with the potential to surpass the Shockley−Quessier efficiency limit. Zhu and co-workers suggested[15,20] that reduced carrier−lattice interactions

Received: May 30, 2017
Accepted: June 29, 2017
Published: June 29, 2017

DOI: 10.1021/acs.jpclett.7b01357
J. Phys. Chem. Lett. 2017, 8, 3211−3215

due to polarons could explain the slow cooling observed in transient absorption[18,19] and time-resolved two-photon photoelectron[20] measurements. Beard and co-workers instead proposed that a hot phonon bottleneck produces the effect. A bottleneck forms when an excited phonon subpopulation relaxes so slowly that, at high excitation densities, it nears thermal equilibrium with hot carriers. This model naturally raises the question of which phonon modes are responsible for a bottleneck, so that phonon engineering approaches (common in the design of thermoelectric materials) might be applied to optimize perovskites for hot carrier photovoltaics. Very recently, Yang et al.[21] suggested that acoustic phonon upconversion could allow energy to be recycled into the lowest-frequency optical phonons, producing the bottleneck.

Here we present 2D electronic spectra (2D-ES) of MAPI thin films at room temperature and covering the energy region near the band edge. The waiting time dynamics show carrier cooling as well as a persistent "warm" carrier population above the band edge. We also observe a long-lived coherent phonon at 0.9 THz, which we identify as potentially responsible for a hot phonon bottleneck. Finally, we observe that the pump frequency resolution in a 2D spectrum allows the photoinduced absorption (PIA) feature due to band gap renormalization to be observed independently from the carrier cooling dynamics.

Figure 1a shows the shape of the MAPI film absorption spectrum near the band edge together with the laser spectrum after it has passed through the sample. A flat laser spectrum covering 1.55−1.75 eV yields a peak in the transmitted light at frequencies below the band edge. Figure 1b shows the laser pulse sequence used to obtain a 2D spectrum. Each 2D plot is obtained by scanning the coherence time τ for a set value waiting time T. The excitation frequency ω_τ is obtained via Fourier transform from the time domain data, while the emission frequency ω_t is measured by a spectrometer. The result is displayed as a 2D time-resolved frequency correlation spectrum, as in Figure 2.

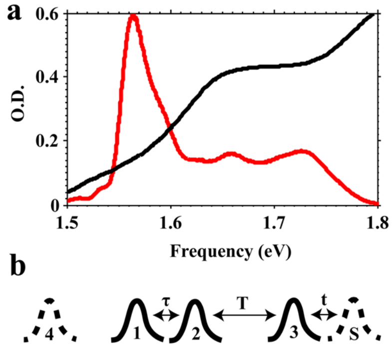

Figure 1. (a) Linear absorption spectrum of a 150 nm thick MAPI film (black) and transmitted laser power spectrum (red), which acts as the local oscillator for heterodyne detection and places limits on the frequencies in the 2D spectrum. At 1.65 eV, the optical density of the film was 0.6. (b) Pulse sequence and time delays for 2D-ES. Pulses 1 and 2 provide pump interactions; pulse 3 is the probe; pulse 4 is the local oscillator used for heterodyne detection; "S" denotes the emitted echo/four-wave mixing signal. We refer to the delays τ and T as coherence time and waiting time, respectively. For a more detailed description of 2D-ES, refer to Brixner et al.[22]

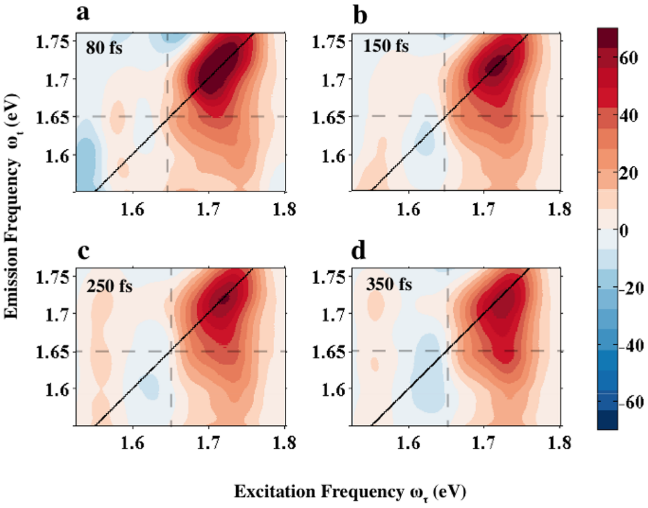

Figure 2. Real (absorptive) 2D spectra of MAPI films at waiting times T = (a) 80, (b) 150, (c) 250, and (d) 350 fs. The black line marks the spectrum diagonal, and the band edge at 1.65 eV is marked with the dashed lines. The positive (bleach) signals are colored red, and negative (PIA) signals are blue. A downward elongation of the main bleach feature results when carriers cool toward the band edge.

Figure 2 shows the real portion of the phased 2D spectra at a progression of waiting times. The initial carrier density is $n = 1.3 \times 10^{18}$ cm^{-3} (see calculations in the Experimental Methods section). The dominant signal is a bleach resulting from absorption at and above the band edge (1.65 eV). Within the first 300 fs, the main peak shifts slightly below the diagonal. This indicates rapid lattice reorganization and/or carrier thermalization, which was very recently investigated with 2D-ES using ultrashort pulses.[23] A broad bleach below the diagonal grows as carriers initially excited above 1.65 eV cool to fill the states along the sloping band edge.

For pump energies below the band gap, we observe a broad PIA feature, which has been previously observed in transient absorption measurements.[18,19] The PIA red of the band edge is attributed to band gap renormalization, a red shift that results when carrier−carrier exchange and correlation interactions lower the valence band energy. This feature is only visible for pump energies below the band gap because at higher pump energies it is canceled by the strongly positive bleach feature. Interestingly, the PIA observed here appears less transient than was observed at the same probe energy in transient absorption. Indeed, a feature due to band gap renormalization should decay on a similar time scale as the carrier population. In transient absorption spectra, the PIA is canceled on a more rapid time scale as the lower diagonal bleach feature associated with hot carrier cooling grows in. The pump frequency resolution in a 2D spectrum therefore allows the bleach and PIA signals to be measured semi-independently.

Figure 3a shows the total absolute-value 2D spectrum taken at waiting time T = 10 ps. The average amplitudes within the boxed areas are plotted in Figure 3b. The red and orange traces show the cross-peak growth associated with carrier cooling, with an exponential rise time of about 300 fs. However, the majority of the carriers remain above the band edge for more than 6 ps, as evidenced by the slow decay of the upper diagonal peak. The bandwidth available in our experiment shows that the slow cooling occurs for carriers with a broad range of energies up to at least 75 meV ($3k_BT$) above the band edge. Though our experiment does not measure hot carriers far above the band gap, the slow cooling that we observe for these "warm" carriers is consistent with that previously observed in transient

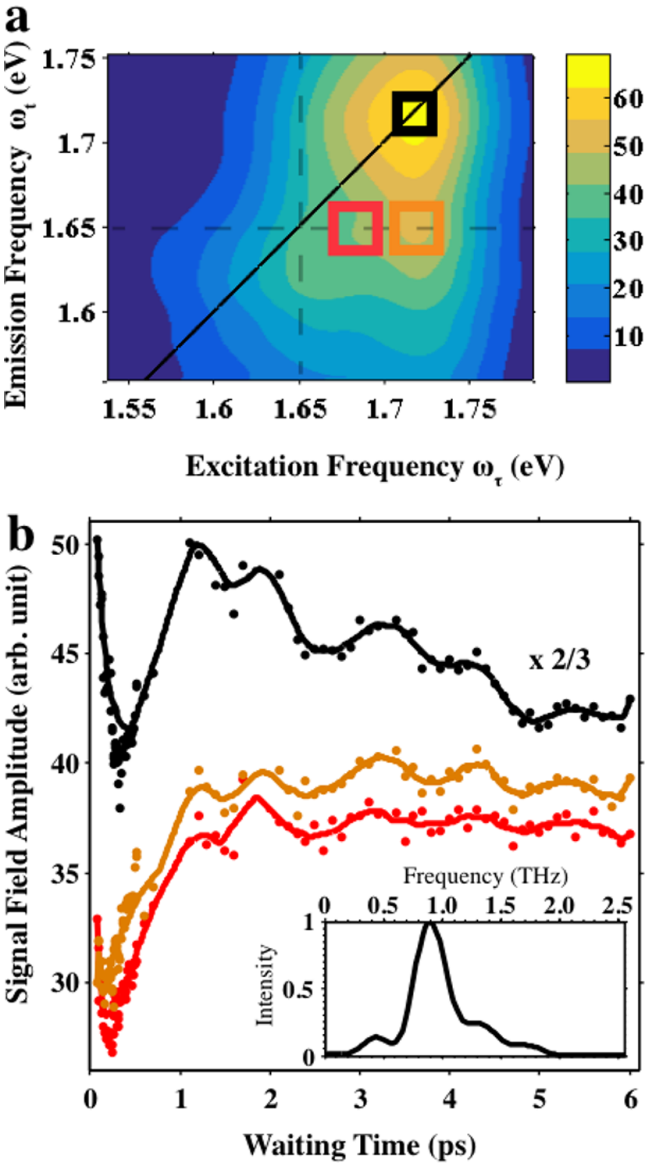

Figure 3. (a) Total (absolute-value) 2D spectrum at T = 10 ps, with boxed regions of interest corresponding to the main diagonal peak above the band edge (black) and two lower cross-peak areas (orange and red). The band edge at 1.65 eV is marked with the dashed lines. (b) Plots over waiting time of the absolute value spectrum amplitude averaged over the different boxed regions shown in (a). Lines to guide the eye have been drawn using a smoothed spline interpolation of the raw data points (also plotted). Amplitude oscillations in the black, red, and orange curves decay with exponential lifetimes of 4, 6, and 18 ps, respectively. The main diagonal peak amplitude plot (black) has been scaled by a factor of 2/3. Inset: Fourier power spectrum of the coherent phonon amplitude oscillations obtained from the spline interpolation of the lower cross-peak trace (orange line) from 2 to 6 ps. Early time data was omitted to remove the zero-frequency component, while the 0.1 ps data interval only adequately samples frequencies up to about 2.5 THz. The peak frequency is at 0.9 THz (30 cm^{-1}, 3.7 meV).

absorption[18,19] and time-resolved two-photon photoelectron[20] measurements.

The traces in Figure 3b show very clear amplitude oscillations, with the same phase and frequency preserved throughout different areas of the 2D spectrum. The Fourier power spectrum of these oscillations peaks strongly at 0.9 THz, as shown in the inset. Such oscillations in the 2D electronic spectrum are caused by the evolution of vibrational wavepackets (phonons), generated through an indirect band gap excitation and interacting with the charge carriers.

The frequency matches that of coherent phonon oscillations recently observed in pump−probe experiments on MAPI films in the orthorhombic phase at 77 K,[24] though not previously seen at room temperature. Because the 2D spectrum measurement is background-free, oscillations can be measured more sensitively than by transient absorption. Moreover, when the signal is integrated over the excitation axis as in transient absorption spectroscopy, small phase differences can attenuate the resulting sum oscillation. We note that the limited range of waiting times measured in this work effectively broadens the Fourier peak, so that the width is not necessarily meaningful.

A collection of modes in the 0.9−1 THz frequency range have been assigned to a set of Pb−I−Pb angular distortions with mixed transverse-longitudinal optical character.[25] This frequency has been previously observed in both Raman[25,26] and THz[25,27] spectra of MAPI in both the orthorhombic and tetragonal phases. In fact, owing to low symmetry in the MAPI structure, phonons cannot be simply assigned to irreducible symmetry groups, and most exhibit both Raman and IR activity.[26] It is therefore interesting that the 2D spectra show no influence from the second prominent collection of optical phonons near 2 THz.[27] These modes were assigned to Pb−I bond stretches and are strongly coupled to the methylammonium tumbling because the cage contractions lead to collisions with the interstitial cation.[28] This is in stark contrast to the Pb−I−Pb angular distortions, which preserve bond length and are essentially uncoupled to the organic cation. That the same coherent phonon oscillations can be observed both in the low-temperature orthorhombic phase[24] (where cation motions are locked) and in the tetragonal phase at room temperature (where cations reorient freely) further indicates that the coherent modes do not couple to the methylammonium cation. We note that observing the organic cation librations themselves (around 5−7 THz) in 2D spectral oscillations would require a greater sampling rate over the waiting time than that used in this work.

The vibrational dephasing times evidenced by the amplitude decay of the 0.9 THz oscillations are remarkably slow. Oscillations on the main diagonal peak (Figure 3b, black) decay with an exponential lifetime of γ^{-1} = 4 ps, while the two lower cross-peak regions show γ^{-1} = 6 ps (Figure 3b, red) and γ^{-1} ≈ 18 ps (orange). By contrast, Leguy et al. estimated a much shorter lifetime of ~100 fs for the 2 THz mode from the Raman line width at 300 K (but did not have sufficient experimental resolution to estimate lifetimes for the modes near 1 THz).[25] The long dephasing times suggest that the 0.9 THz optical phonon(s) that we observe has a strong coupling to the electronic transition but weak interactions with the remainder of the phonon modes, especially compared to the 2 THz mixed organic−inorganic mode. The strong coupling between the inorganic-only phonon and the electronic transition is consistent with a calculation by Kawai et al.[29] predicting that charge carriers couple mainly to the lattice and only indirectly to the interstitial cation because the valence and conduction band states involved in the near-band edge transitions consist of only I and Pb orbitals. However, an isotopic substitution study by Gong et al. demonstrated that carrier lifetimes indeed depend on the cation libration frequency.[30] Together with the absence of persistent hot carriers in the all-inorganic perovskite

$CsPbBr_3$,[16] this suggests that the organic cation still plays a key role. The following picture emerges: electronic transitions and free charge carriers interact on the shortest time scales only with the inorganic lattice phonons, especially a low-frequency mode involving only angular distortions. On longer time scales, the organic cation begins to have an indirect influence on the charge carriers via the coupling between cation rotations and lattice stretching modes. If a large portion of the initial energy lost to the lattice is deposited in the coherent 0.9 THz mode(s), isolated from the rest of the lattice, a bottleneck could form.

Because MAPI films have poor thermal conductivity, suggesting strongly scattered and/or highly localized acoustic phonons, it is tempting to think that acoustic phonons might be responsible for the bottleneck effect. However, our observation of coherent phonon oscillations is evidence contrary to the recent suggestion that the bottleneck is due to acoustic phonon up-conversion[21] because a cooling and up-conversion cycle would not preserve the phonon phase coherence. Therefore, if up-conversion into the low-energy optical phonons contributes to the bottleneck effect, it is only on time scales greater than ~10 ps.

Understanding the interaction of optical excitations and charge carriers with the nuclear motions of the lattice is critical to unraveling the puzzle of perovskites' remarkable photovoltaic properties. The enhanced resolution afforded by two energy axes in two-dimensional electronic spectra clearly reveals the coupling between the electronic transition and a coherent 0.9 THz optical phonon(s) in MAPI. It seems likely that the electrons also couple strongly to these motions, which in turn interact weakly with the rest of the phonon bath, making it a good candidate as the origin of a phonon bottleneck. Modes near 0.9 THz mode are assigned to Pb−I−Pb angular distortions, which do not couple to the methylammonium cation reorientations. Despite the striking difference in both charge carrier relaxation and cation rotational freedom between the tetragonal and orthorhombic forms, what is not clear is whether the methylammonium cation interacts with the charge carriers on time scales relevant to the electron cooling.

■ EXPERIMENTAL METHODS

Methylammonium Lead Iodide (MAPI) Films. To fabricate 150 nm thick MAPI films, a two-step method was adopted. The 0.2 M PbI_2 in *N,N*-dimethylformamide (DMF) was spin-coated at 4000 rpm onto the glass substrate and then heated at 75 °C for 5 min. The perovskite film was grown by dipping the PbI_2 film for 1 min in a 8 mg mL^{-1} solution of methylammonium iodide in 2-propanol at a temperature of 75 °C. The substrate was then dried by heating on a hot plate to 100 °C for 10 min. All of the processes were carried out in a N_2-filled glovebox. Samples were exposed briefly to air when transferring to a N_2-filled optical cryostat for the spectroscopic experiments.

Two-Dimensional Electronic Spectroscopy. Broad-band laser pulses were prepared by pumping a home-built noncollinear optical parametric amplifier with a 1 kHz amplified Ti:Sapph laser (Coherent Inc., Astrella). The pulses were compressed to 80 fs using a pair of fused silica prisms, as measured via autocorrelation on a two-photon photodiode at the sample position. The beams were attenuated to achieve a fluence of 4.2 $\mu J/cm^2$ for each pump beam and 0.9 $\mu J/cm^2$ for the probe beam at the sample position. Using the equation $n_0 = \frac{(1 - T - R) \times \phi}{h\nu \times l}$ (transmission $T = 10^{-0.6}$; reflection R = 11%; total pump fluence ϕ = 8.2 $\mu J/cm^2$; photon energy $h\nu$ = 1.65 eV; film thickness l = 150 nm), we calculate the excitation density $n_0 = 1.3 \times 10^{18}$ cm^{-3}.

The phase-stable two-dimensional 2D-ES experimental arrangement used in this work has been described elsewhere.[22] A combination of a beam splitter and diffractive optic were used to generate four beams in a box-car geometry. The waiting time delay T between the pump and probe was controlled using a motorized delay stage, while the delay τ between the two pump pulses was controlled by translating 4° glass wedge pairs placed in the beam path. The four beams were focused to a $1/e^2$ diameter of 60 μm and carefully overlapped at the sample position. The signal was then emitted along the phase-matched direction, co-propagating with the attenuated local oscillator beam. The heterodyned four-wave mixing signal was detected in the frequency domain using a spectrometer (Princeton Instruments, Acton Advanced SP2300A) and CCD camera (Princeton Instruments, PIXIS 100). A linear phase correction corresponding to the time delay between the signal and local oscillator was added to generate the approximately phased spectra in Figure 2. Amplitude oscillations were measured using the absolute value spectra (see Figure 3) in order to rule out any possible artifact from the phasing procedure.

The MAPI samples are much more scattered than a typical single crystal or nanocrystal solution, which poses a significant experimental challenge in 2D-ES. Two choppers and an economical microcontroller (Arduino Uno) were used to dynamically remove undesired scattered light, especially the scattered probe interference with the local oscillator. This contribution is especially important to remove because the probe-local oscillator delay is nearly equal to the signal-local oscillator delay; therefore, it is not easily removed using a time domain window during the data processing. A detailed description of this scheme for significantly improving the signal-to-noise ratio can be found in ref 31, in which a frequency-resolved pump−probe measurement was used for demonstration.

■ AUTHOR INFORMATION

ORCID

Peidong Yang: 0000-0003-4799-1684
Graham R. Fleming: 0000-0003-0847-1838

Notes

The authors declare no competing financial interest.

■ ACKNOWLEDGMENTS

This material is based upon work supported by the National Science Foundation under CHE-1362830. The sample preparation work in the Yang group was supported by the U.S. Department of Energy, Office of Science, Basic Energy Sciences, Materials Sciences and Engineering Division under Contract No. DE-AC02-05CH11231 (PChem KC3103). D.M.M. received a National Science Foundation Graduate Research Fellowship under Grant No. DGE-1106400.

■ REFERENCES

(1) Herz, L. M. Charge-Carrier Dynamics in Organic-Inorganic Metal Halide Perovskites. *Annu. Rev. Phys. Chem.* **2016**, *67*, 65−89.

(2) Bi, Y.; Hutter, E. M.; Fang, Y.; Dong, Q.; Huang, J.; Savenije, T. J. Charge Carrier Lifetimes Exceeding 15 Ms in Methylammonium Lead Iodide Single Crystals. *J. Phys. Chem. Lett.* **2016**, *7* (5), 923−928.

(3) Ponseca, C. S.; Savenije, T. J.; Abdellah, M.; Zheng, K.; Yartsev, A.; Pascher, T.; Harlang, T.; Chabera, P.; Pullerits, T.; Stepanov, A.;

et al. Organometal Halide Perovskite Solar Cell Materials Rationalized: Ultrafast Charge Generation, High and Microsecond-Long Balanced Mobilities, and Slow Recombination. *J. Am. Chem. Soc.* **2014**, *136* (14), 5189−5192.

(4) Chen, Y.; Yi, H. T.; Wu, X.; Haroldson, R.; Gartstein, Y.; Zakhidov, A.; Zhu, Z.-Y.; Podzorov, V.; et al. Extended Carrier Lifetimes and Diffusion in Hybrid Perovskites Revealed by Hall Effect and Photoconductivity Measurements. *Nat. Commun.* **2016**, *7*, 12253.

(5) Stranks, S. D.; Stranks, S. D.; Eperon, G. E.; Grancini, G.; Menelaou, C.; Alcocer, M. J. P.; Leijtens, T.; Herz, L. M.; Petrozza, A.; Snaith, H. J.; et al. Electron-Hole Diffusion Lengths Exceeding 1 Micrometer in an Organometal Trihalide Perovskite Absorber. *Science* **2013**, *342* (2013), 341−344.

(6) Xing, G.; Mathews, N.; Lim, S. S.; Lam, Y. M.; Mhaisalkar, S.; Sum, T. C.; et al. Long-Range Balanced Electron- and Hole-Transport Lengths in Organic-Inorganic CH3NH3PbI3. *Science* **2013**, *342*, 344−347.

(7) Deschler, F.; Price, M.; Pathak, S.; Klintberg, L. E.; Jarausch, D.; Higler, R.; Leijtens, T.; Stranks, S. D.; Snaith, H. J.; Phillips, R. T.; et al. High Photoluminescence Efficiency and Optically Pumped Lasing in Solution-Processed Mixed Halide Perovskite Semiconductors. *J. Phys. Chem. Lett.* **2014**, *5*, 1421−1426.

(8) Zhu, H.; Fu, Y.; Meng, F.; Wu, X.; Gong, Z.; Ding, Q.; Gustafsson, M. V.; Trinh, M. T.; Jin, S.; Zhu, X.-Y. Lead Halide Perovskite Nanowire Lasers with Low Lasing Thresholds and High Quality Factors. *Nat. Mater.* **2015**, *14* (6), 636−642.

(9) Filippetti, A.; Caddeo, C.; Delugas, P. D.; Mattoni, A. On the Appealing Perspectives of Hybrid Lead-Iodide Perovskites as Thermoelectric Materials. *J. Phys. Chem. C* **2016**, *120*, 28472−28479.

(10) Nagabhushana, G. P.; Shivaramaiah, R.; Navrotsky, A. Direct Thermochemical Verification of Thermodynamic Instability of Lead Halide Perovskites. *Proc. Natl. Acad. Sci. U. S. A.* **2016**, *113* (28), 7717−7721.

(11) Boix, P. P.; Agarwala, S.; Koh, T. M.; Mathews, N.; Mhaisalkar, S. G. Perovskite Solar Cells: Beyond Methylammonium Lead Iodide. *J. Phys. Chem. Lett.* **2015**, *6* (5), 898−907.

(12) Miyata, A.; Mitioglu, A.; Plochocka, P.; Portugall, O.; Wang, J. T.; Stranks, S. D.; Snaith, H. J.; Nicholas, R. J. Direct Measurement of the Exciton Binding Energy and Effective Masses for Charge Carriers in Organic-Inorganic Tri-Halide Perovskites. *Nat. Phys.* **2015**, *11* (7), 582−587.

(13) D'Innocenzo, V.; Grancini, G.; Alcocer, M. J. P.; Kandada, A. R. S.; Stranks, S. D.; Lee, M. M.; Lanzani, G.; Snaith, H. J.; Petrozza, A. Excitons versus Free Charges in Organo-Lead Tri-Halide Perovskites. *Nat. Commun.* **2014**, *5*, 3586.

(14) Wang, H.; Whittaker-Brooks, L.; Fleming, G. R. Exciton and Free Charge Dynamics of Methylammonium Lead Iodide Perovskites Are Different in the Tetragonal and Orthorhombic Phases. *J. Phys. Chem. C* **2015**, *119* (34), 19590−19595.

(15) Zhu, X. Y.; Podzorov, V. Charge Carriers in Hybrid Organic-Inorganic Lead Halide Perovskites Might Be Protected as Large Polarons. *J. Phys. Chem. Lett.* **2015**, *6* (23), 4758−4761.

(16) Zhu, H.; Miyata, K.; Fu, Y.; Wang, J.; Joshi, P.; Niesner, D.; Williams, K. W.; Jin, S.; Zhu, X.-Y. Screening in Crystalline Liquids Protects Energetic Carriers in Hybrid Perovskites. *Science* **2016**, *353* (6306), 1409−1413.

(17) Bakulin, A. A.; Selig, O.; Bakker, H. J.; Rezus, Y. L. A.; Müller, C.; Glaser, T.; Lovrincic, R.; Sun, Z.; Chen, Z.; Walsh, A.; et al. Real-Time Observation of Organic Cation Reorientation in Methylammonium Lead-Iodide Perovskites. *J. Phys. Chem. Lett.* **2015**, *6*, 3663−3669.

(18) Price, M. B.; Butkus, J.; Jellicoe, T. C.; Sadhanala, A.; Briane, A.; Halpert, J. E.; Broch, K.; Hodgkiss, J. M.; Friend, R. H.; Deschler, F. Hot-Carrier Cooling and Photoinduced Refractive Index Changes in Organic−inorganic Lead Halide Perovskites. *Nat. Commun.* **2015**, *6* (May), 8420.

(19) Yang, Y.; Ostrowski, D. P.; France, R. M.; Zhu, K.; van de Lagemaat, J.; Luther, J. M.; Beard, M. C. Observation of a Hot-Phonon Bottleneck in Lead-Iodide Perovskites. *Nat. Photonics* **2015**, *10*, 53−59.

(20) Niesner, D.; Zhu, H.; Miyata, K.; Joshi, P. P.; Evans, T. J. S.; Kudisch, B. J.; Trinh, M. T.; Marks, M.; Zhu, X. Persistent Energetic Electrons in Methylammonium Lead Iodide Perovskite Thin Films. *J. Am. Chem. Soc.* **2016**, *138* (48), 15717−15726.

(21) Yang, J.; Wen, X.; Xia, H.; Sheng, R.; Ma, Q.; Kim, J.; Tapping, P.; Harada, T.; Kee, T. W.; Huang, F.; et al. Acoustic-Optical Phonon up-Conversion and Hot-Phonon Bottleneck in Lead-Halide Perovskites. *Nat. Commun.* **2017**, *8*, 14120.

(22) Brixner, T.; Mancal, T.; Stiopkin, I. V.; Fleming, G. R. Phase-Stabilized Two-Dimensional Electronic Spectroscopy. *J. Chem. Phys.* **2004**, *121* (9), 4221−4236.

(23) Richter, J. M.; Branchi, F.; Camargo, F. V.; de Almeida Camargo, F. V.; Zhao, B.; Friend, R. H.; Cerullo, G.; Deschler, F. Ultrafast Carrier Thermalization in Lead Iodide Perovskite Probed with Two-Dimensional Electronic Spectroscopy. arXiv:1701.03919. arXiv.org e-Print archive. https://arxiv.org/abs/1701.03919 (accessed May 30, 2017).

(24) Wang, H.; Valkunas, L.; Cao, T.; Whittaker-Brooks, L.; Fleming, G. R. Coulomb Screening and Coherent Phonon in Methylammonium Lead Iodide Perovskites. *J. Phys. Chem. Lett.* **2016**, *7*, 3284−3289.

(25) Leguy, A. M. A.; Goñi, A. R.; Frost, J. M.; Skelton, J.; Brivio, F.; Rodríguez-Martínez, X.; Weber, O. J.; Pallipurath, A.; Alonso, M. I.; Campoy-Quiles, M.; et al. Dynamic Disorder, Phonon Lifetimes, and the Assignment of Modes to the Vibrational Spectra of Methylammonium Lead Halide Perovskites. *Phys. Chem. Chem. Phys.* **2016**, *18* (39), 27051−27066.

(26) Brivio, F.; Frost, J. M.; Skelton, J. M.; Jackson, A. J.; Weber, O. J.; Weller, M. T.; Goni, A. R.; et al. Lattice Dynamics and Vibrational Spectra of the Orthorhombic, Tetragonal, and Cubic Phases of Methylammonium Lead Iodide. *Phys. Rev. B: Condens. Matter Mater. Phys.* **2015**, *92*, 144308.

(27) La-O-Vorakiat, C.; Xia, H.; Kadro, J.; Salim, T.; Zhao, D.; Ahmed, T.; Lam, Y. M.; Zhu, J. X.; Marcus, R. A.; Michel-Beyerle, M. E.; et al. Phonon Mode Transformation Across the Orthohombic-Tetragonal Phase Transition in a Lead Iodide Perovskite CH3NH3PbI3: A Terahertz Time-Domain Spectroscopy Approach. *J. Phys. Chem. Lett.* **2016**, *7* (1), 1−6.

(28) Pérez-Osorio, M. A.; Milot, R. L.; Filip, M. R.; Patel, J. B.; Herz, L. M.; Johnston, M. B.; Giustino, F. Vibrational Properties of the Organic-Inorganic Halide Perovskite CH3NH3PbI3 from Theory and Experiment: Factor Group Analysis, First-Principles Calculations, and Low-Temperature Infrared Spectra. *J. Phys. Chem. C* **2015**, *119* (46), 25703−25718.

(29) Kawai, H.; Giorgi, G.; Marini, A.; Yamashita, K. The Mechanism of Slow Hot-Hole Cooling in Lead-Iodide Perovskite: First-Principles Calculation on Carrier Lifetime from Electron-Phonon Interaction. *Nano Lett.* **2015**, *15* (5), 3103−3108.

(30) Gong, J.; Yang, M.; Ma, X.; Schaller, R. D.; Liu, G.; Kong, L.; Yang, Y.; Beard, M. C.; Lesslie, M.; Dai, Y.; et al. Electron-Rotor Interaction in Organic-Inorganic Lead Iodide Perovskites Discovered by Isotope Effects. *J. Phys. Chem. Lett.* **2016**, *7* (15), 2879−2887.

(31) Guo, L.; Monahan, D. M.; Fleming, G. Rapid and Economical Data Acquisition in Ultrafast Frequency-Resolved Spectroscopy Using Choppers and a Microcontroller. *Opt. Express* **2016**, *24*, 18126−18132.

DOI: 10.1021/acs.jpclett.7b01357
J. Phys. Chem. Lett. 2017, 8, 3211−3215